International Journal of Multiphase Flow 196 (2026) 105556

Contents lists available at ScienceDirect

International Journal of Multiphase Flow

journal homepage: www.elsevier.com/locate/ijmulflow

Research Paper

Impact of variability in inlet operating conditions on CO_2 transport in pipelines

Davide Picchi [a],*, Valentina Ciriello [b]

[a] Department of Mechanical and Industrial Engineering, Università degli Studi di Brescia, Brescia 25123, Italy
[b] Department of Civil, Chemical, Environmental, and Materials Engineering, University of Bologna, Bologna 40136, Italy

HIGHLIGHTS

- We propose a comprehensive stochastic framework to study CO_2 transport in pipelines.
- We quantify the role of operational parameters in avoiding two-phase flow conditions.
- The inlet pressure and velocity are the most influential parameters.

GRAPHICAL ABSTRACT

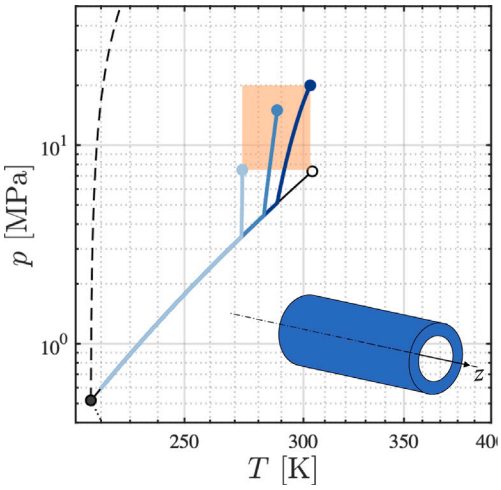

ARTICLE INFO

Keywords:
CO_2 transport
Homogeneous equilibrium model
Polynomial Chaos Expansion
Global sensitivity analysis
Uncertainty quantification
Carbon Capture and Storage

ABSTRACT

The success of CCS technologies relies on the effectiveness and safety of the infrastructure for the transport of carbon dioxide in pressurized pipelines. Unlike natural gas networks, long-distance carbon dioxide transport presents critical design challenges, such as the need for repressurization to prevent two-phase flow conditions and potential freezing. To address this, we propose a comprehensive assessment framework that combines high-fidelity numerical simulations with a stochastic approach based on the Polynomial Chaos Expansion (PCE). Specifically, we employ the Homogeneous Equilibrium Model (HEM) to compute key quantities of interest (QoIs) — related to pressure drop and the maximum distance before repressurization is required — under a design scenario inspired by the Cortez pipeline (Colorado, USA). Based on PCE surrogates, we then perform global sensitivity analyses and uncertainty quantification to evaluate how variability in inlet parameters influences these QoIs, mapping results across a range of realistic operating conditions. Our results provide critical insight into the risks connected with CO_2 transport and support the optimal design of operating conditions. Moreover, the proposed methodology is general and easily applicable to other CO_2 transport facilities.

* Corresponding author.
E-mail addresses: davide.picchi@unibs.it (D. Picchi), v.ciriello@unibo.it (V. Ciriello).

https://doi.org/10.1016/j.ijmultiphaseflow.2025.105556
Received 19 August 2025; Received in revised form 30 October 2025; Accepted 22 November 2025
Available online 28 November 2025

1. Introduction

Carbon Capture and Storage (CCS) technologies aim to take approximately 85%–90% of CO_2 emissions and securely store it in depleted oil reservoirs or saline aquifers beneath the earth's surface (Metz et al., 2005; Zhang et al., 2022). To achieve the climate objectives set forth by the Energy Union for 2050 and the Paris Agreement, it is essential to transport carbon dioxide from production to storage sites in pressurized pipelines (see e.g., Brown et al., 2015; Munkejord et al., 2016; Edwards and Celia, 2018; Onyebuchi et al., 2018; Peletiri et al., 2018; Vitali et al., 2022).

Unfortunately, the annual transportation of carbon dioxide in pipelines remains limited to only a few megatons, primarily in enhanced oil recovery operations (Orr and Taber, 1984; Blunt et al., 1993; Abedini and Torabi, 2014; Yu et al., 2015; Jia et al., 2019). For instance, in the United States, the existing CO_2 infrastructure (about 6000 km) is quite modest compared to the natural gas network (Koornneef et al., 2010). Moreover, carbon dioxide exhibits different characteristics than natural gas, necessitating a redefinition of the minimum operating conditions to fulfill safety standards. The natural gas infrastructure is designed to operate in a gaseous state and, therefore, it cannot be directly converted to operate with carbon dioxide since, at the natural gas design conditions, CO_2 exists in a dense liquid or supercritical state. The critical temperature of pure CO_2 (31.1 °C) is close to ambient temperature and, therefore, the transition to two-phase flow due to phase change (also in the case of carbon dioxide mixtures) can significantly impact the safety and efficiency of the facilities (de Visser et al., 2008; Li et al., 2011; Onyebuchi et al., 2018). This would significantly increase the pressure drop and the pumping costs and, eventually, lead to onset of slug flow threatening the pipe integrity due to large fluctuations in the local mass flux and dynamics stresses (see e.g., Bendiksen and Espedal (1992) and Bamidele et al. (2021)).

Pipelines, in fact, are generally designed to operate with CO_2 in a dense liquid or supercritical state, which presents significant design challenges, including the selection of operating conditions and the distance before repressurization. Accidents, such as leaks from pipelines caused by pipe fractures, can significantly alter the fluid pressure. This would potentially initiate the transition to two-phase flow conditions (Munkejord et al., 2020a) affecting both transport safety and efficiency and resulting in a temperature drop that makes the pipe material vulnerable to cracking (see e.g., Pham and Rusli, 2016; Mahgerefteh et al., 2016; Skarsvåg et al., 2023).

An additional challenge in the optimal design of CO_2 pipelines is that, differently from the natural gas infrastructure often situated in low populated regions, the large-scale CCS network will be probably located in regions that are highly populated (Koornneef et al., 2010). This scenario necessitates a comprehensive and robust assessment of safety and risks that may affect residents living near the pipelines. In other words, quantifying the probability of pipeline failures under both design and off-design conditions is essential for the success of the CCS infrastructure.

These open challenges require engineering tools capable of predicting the flow characteristics and able to capture the transition to two-phase flow conditions. Due to their computational burden, CFD simulations are not affordable for a pipeline with realistic dimensions and, therefore, the common practice is to use a simplified approach. Specifically, the common strategy is to treat the problem by averaging the conservation laws in space in time to obtain a simplified one-dimensional model. Then, the physical information that is inevitably lost during this averaging process, is enforced via *ad hoc* closure relations. This family of models has been adopted since long in the nuclear and oil and gas industry, and, only recently, adapted to the case transport of CO_2. Examples are the Homogeneous Equilibrium model (see e.g., Brown et al. (2014), Lu and Connell (2014), Fang et al. (2019) and Angielczyk et al. (2020)), the Drift model (see e.g., Lu and Connell (2008) and Aursand et al. (2013)), the Two-fluid model (Drew, 1983; Hammer and Morin, 2014; Munkejord and Hammer, 2015; Linga and Lund, 2016; Munkejord et al., 2020b), and the simplified (or pressure free) Two-fluid model (Bonzanini et al., 2017; Sanderse et al., 2021; Buist et al., 2022, 2023, 2024). A comprehensive description of these one-dimensional models is presented in Städtke (2006).

In this paper, we model CO_2 transport with the steady state Homogeneous Equilibrium model and focus on a set of quantities of interest (QoIs) computed by the model that are the characteristics of the flow along the pipeline, i.e., the velocity, pressure, and temperature, and the locations where the transition from single-phase to two-phase condition takes place, and where the carbon dioxide reaches the triple point. If the former defines the necessity for repressurization, the latter is linked to a freezing of carbon dioxide inside the pipeline which may increase the risk of a pipe failure. Although it assumes that the phases are perfectly mixed and neglects the different two-phase flow regimes, we adopt the homogeneous model because, to the best of our knowledge, flow-regime specific closures for the frictional pressure gradient and flow pattern maps are still not available for the case of carbon dioxide in large diameter pipes. Among the outputs of the model, we will focus primarily on identifying occurrence of two phase flow and the positioning of repressurization stations.

Differently from previous works on the topic, where the design of boosting or repressurization station are examined in a deterministic way using commercially available simulator (just to mention a few, Zhang et al., 2006; Teh et al., 2015; Munkejord et al., 2013; Witkowski et al., 2013) or simple friction loss estimation (e.g., Chandel et al., 2010), our goal is to couple high-fidelity numerical simulations (in our case represented by the HEM predictions) with a probabilistic approach capable of performing global sensitivity analysis and uncertainty quantification at negligible computational cost, while mapping the QoIs in the parameter space using only a limited number of high-fidelity simulations.

Starting from a defined design scenario inspired by the Cortez pipeline, which supplies CO_2 from the McElmo Dome (Colorado, USA) to Denver crossing the Rocky Mountains (Metz et al., 2005), we investigate the effect of the variability of the boundary conditions at the inlet, mimicking the operation conditions, on the QoIs. Specifically, we develop two different analyses. We first focus on the locations where the transition to two-phase flow occurs, and where the carbon dioxide reaches the triple point, by performing Global Sensitivity Analysis (GSA) and mapping these quantities on a range of realistic operating conditions. Secondly, we consider a variability at the inlet around the average operating condition to compute the statistics of flow characteristics. We do so to discover how variability in key governing conditions impacts the variability in the QoIs to (i) ultimately narrow down the number of conditions to focus on, and (ii) provide a method to design appropriate operating conditions.

To facilitate GSA, uncertainty quantification, and the mapping of the QoIs in the space of variability of inlet parameters, we employ surrogates based on the Polynomial Chaos Expansion (PCE) method (Xiu and Karniadakis, 2002). PCE requires only a minimal number of high-fidelity simulations to effectively reproduce the response surface of the QoIs if the number of parameters is relatively low. This is a key advantage with respect to neural networks, which are attractive for their ability to handle high-dimensional input–output mappings, but whose effectiveness depends on the availability of large training datasets, making their deployment advantageous only if the training phase is less computationally demanding than performing the full set of ensemble-based computations for GSA and uncertainty quantification (Chiofalo et al., 2025).

The PCE approximation is expressed as a polynomial series, which incurs a negligible computational cost. As a result, we can conduct ensemble-based computations, making this method more advantageous than traditional Monte Carlo simulations (Ciriello et al., 2017). In particular, it has been demonstrated that GSA can be performed through analytical post-processing of PCE coefficients to derive variance-based

metrics (Sudret, 2008) and distribution-based metrics (Ciriello et al., 2019). Our work demonstrates that HEM model predictions and PCE surrogates can be effectively integrated to obtain accurate and robust results with minimal computational effort. In particular, the ability to map the QoIs with PCE across the space of variability of the governing parameters enhances physical understanding and supports decision-making. As such, our approach has the potential to assist field engineers in assessing uncertainty and guiding the design of pipelines for the long-distance transport of carbon dioxide.

The paper is organized as follows. In Section 2, we present the homogeneous equilibrium model to simulate single and two phase flow of carbon dioxide in pipelines. In Section 3, we introduce the test case scenario and describe the PCE method used to carry out uncertainty quantification and global sensitivity analyses. In Section 4 we discuss the results. Finally, a set of conclusions closes the paper.

2. The Homogeneous Equilibrium Model (HEM) for CO_2 transport in pipelines

In this work, we model the flow of carbon dioxide in a pipeline of diameter D and length L using the one-dimensional Homogeneous Equilibrium Model (HEM) (Städtke, 2006). Specifically, we consider a pipeline that is sufficiently long, $L \gg D$, so that the conservation laws are expressed in terms of cross-section averaged thermodynamic variables. At the steady state, the balance of mass, momentum, and energy yields to

$$u\frac{d\rho}{dz} + \rho\frac{du}{dz} = 0, \tag{1}$$

$$\rho u\frac{du}{dz} = -\frac{dp}{dz} - \frac{\tau S}{A} + \rho g \sin\beta, \tag{2}$$

$$\rho u\frac{dh}{dz} + \rho u^2\frac{du}{dz} = -\frac{qS}{A} + \rho u g \sin\beta, \tag{3}$$

where $S = \pi D$, $A = \pi D^2/4$, τ, q are the internal perimeter, the cross-section area, the mean wall shear, and the specific heat flux exchanged between the fluid and the environment; β is the pipe inclination with respect to the horizontal, positive when the pipe is inclined downward. Eqs. (1)–(3) are a set of three equations with 5 unknowns (i.e., the density $\rho(z)$, the fluid velocity $u(z)$, the pressure $p(z)$, the fluid enthalpy h, and the fluid temperature $T(z)$) that need to be closed using an equation of state. In the following sections, we present the model closures for the case of single-phase and two-phase flow conditions, respectively.

2.1. Single-phase flow

When carbon dioxide is single phase (i.e., liquid, gas, or supercritical) the governing equations are closed using an equation of state in the form $v = v(p,T)$ or, alternatively, $p = p(\rho,T)$ (Gyftopoulos and Beretta, 2005). Specifically, the governing equations Eqs. (1)–(3) are closed using the total differentials of the equation of state and the differential of enthalpy given by

$$\frac{dv}{dz} = \alpha_p v\frac{dT}{dz} - \kappa_T v\frac{dp}{dz}, \tag{4}$$

$$\frac{dh}{dz} = c_p\frac{dT}{dz} + (1 - T\alpha_p)v\frac{dp}{dz}, \tag{5}$$

where $c_p(T,p)$ is the specific heat at constant pressure, while $\alpha_p(T,p)$ and $\kappa_T(T,p)$ are the coefficients of isobaric expansion and isothermal compressibility, respectively, defined as

$$\alpha_p = \frac{1}{v}\left(\frac{\partial v}{\partial T}\right)_p \qquad \kappa_T = -\frac{1}{v}\left(\frac{\partial v}{\partial p}\right)_T. \tag{6}$$

In this work, we use the Peng and Robinson (1976) EoS to describe the thermodynamic properties of carbon dioxide, see Appendix A for details. This equation of state satisfactorily predicts the properties of carbon dioxide in the range of temperatures and pressures typical of carbon dioxide transport while retaining the simplicity of the functional form. This choice does not prevent the reader from considering more sophisticated EoS, such as the one proposed by Reynolds (1979) or the well-known (Span and Wagner, 1996) EoS.

Thus, the single-phase HEM consists in five governing equations, Eqs. (1)–(3) and Eqs. (4)–(5) with five independent variables (i.e., u, ρ, p, h, T).

2.2. Two-phase flow

When carbon dioxide is in a two-phase vapor–liquid state, the HEM assumes that the liquid and vapor are at thermodynamic equilibrium, i.e., temperatures, pressures, and velocities of both phases are equal and can be treated as a mixture. Specifically, the mixture volume and the enthalpy are given by

$$v = \rho^{-1} = v_f + x v_{fg}, \tag{7}$$

$$h = h_f + x h_{fg}, \tag{8}$$

where x is the vapor quality, $v_f(p)$ and $h_f(p)$ are the specific volume and enthalpy of saturated liquid, $v_{fg}(p)$ and $h_{fg}(p)$ the specific volume and enthalpy of vaporization, respectively. Since in two-phase states, p and T are related through the relation $T = T_{sat}(p)$, we express the vaporization properties as functions of the pressure alone.

Using Eqs. (7) and (8), we can recast the mass and energy conservation laws, Eqs. (1) and (3) in terms of derivatives of x, p, and u as

$$\frac{1}{v}\frac{du}{dz} - \frac{u}{v^2}\left[v_{fg}\frac{dx}{dz} + \frac{dp}{dz}\left(\frac{dv_f}{dp} + x\frac{dv_{fg}}{dp}\right)\right] = 0, \tag{9}$$

$$\frac{u^2}{v}\frac{du}{dz} + \frac{u}{v}\left[h_{fg}\frac{dx}{dz} + \frac{dp}{dz}\left(\frac{dh_f}{dp} + x\frac{dh_{fg}}{dp}\right)\right] = -\frac{qS}{A} + \frac{ug}{v}\sin\beta. \tag{10}$$

where the derivative of vaporization properties with respect to pressure are known quantities once the equation of state of the pure substance is known. Thus, the two-phase HEM consists in three governing equations, Eqs. (9), (2) and (10), where the independent variables are the vapor quality, the pressure and the mixture velocity only, i.e., (x,p,u). Note that the model has to be supplemented with explicit expressions for the vaporization properties obtained from the EoS using the Maxwell equal area rule (Klein and Nellis, 2011).

2.3. Model closures

At single-phase flow conditions, the wall shear stress on the r.h.s. of the momentum balance, Eq. (2), is modeled using the Blasius empirical model for the friction factor, f, as

$$\tau = f\frac{\rho u^2}{2} \qquad \text{where} \qquad f = \frac{c}{Re^m} \qquad Re = \frac{\rho u D}{\mu}, \tag{11}$$

where Re is the Reynolds number. The constants in the friction factor formula are chosen depending on the Reynolds number Re, defined in Eq. (11) where $\rho(T,p)$ is the density of pure carbon dioxide while $\mu(T,p)$ is the dynamic viscosity estimated using the model proposed by Fenghour et al. (1998) that has been shown to be very accurate in the range $200\,\text{K} \le T \le 1500\,\text{K}$ up to pressures of 300 MPa. Specifically, when the flow is laminar, (i.e., $Re < 2100$), $f = 16/Re$ and, therefore, $c = 16$ and $m = 1$; instead, when the flow is turbulent (i.e., $Re > 2100$), we adopt the Blasius correlation (Blasius, 1913) with $c = 0.079$ and $m = 0.25$. The transition from laminar to turbulent flow is set at a critical Reynolds number $Re = 2100$ only for the sake of simplicity. In general, although more sophisticated models could be used, such as the Colebrook–White model (Colebrook et al., 1937), we prefer to keep the closures as simpler as possible and to focus on the coupling between the homogeneous model and the stochastic approach that will be discussed later on.

At two-phase flow conditions, determining the frictional pressure gradients requires prior knowledge of the two-phase flow regime, i.e., stratified, core-annular, slug, or dispersed flow regime. Although

the identification of two-phase flow pattern maps and shear stress closures has been an area of research in the scientific community for decades (see e.g., Wallis, 1969; Barnea, 1987; Picchi and Poesio, 2016), this information is still not available for carbon dioxide and remains an ongoing subject of investigation (see e.g., Yun and Kim, 2004; Schmid et al., 2022; Lu and Connell, 2008, 2014). Different flow regimes, in fact, result in different closure relationship for the pressure gradient. For example, an accurate estimation of the pressure drop for slug flows requires knowledge on intermittent flow parameters, i.e., slug frequency, averaged slug length and speed (Taitel and Barnea, 1990; Brauner and Ullmann, 2004; Orell, 2005), for dispersed flows it is necessary to estimate the bubble size distribution and the interaction with the dispersed phase (Angeli and Hewitt, 1999; Picchi et al., 2015), while for stratified and annular flow regimes an accurate model for the interfacial interaction is recommended (Andritsos and Hanratty, 1987; Andreussi and Persen, 1987; Ullmann and Brauner, 2006). In addition to that, adopting flow regime based closures requires a flow pattern map or a robust model to predict flow pattern transition so that the regimes could be chosen depending on the local flow rates. Unfortunately, for the case of carbon dioxide in large diameter pipes either *ad hoc* flow-regimes closures and flow pattern maps are still not available, and, therefore we model the two-phase flow as an homogeneous mixture. Specifically, we assume that liquid and vapor are perfectly mixed, modeling the friction factor in analogy with single phase flow using Eq. (11) where the Reynolds number is evaluated based on mixture properties. Specifically, the mixture density is provided in Eq. (7) while, among the viscosity models available in the literature (see for example, Einstein, 1906; McAdams et al., 1942; Dukler et al., 1964; Lin et al., 1991), we use the one proposed by Cicchitti et al. (1959)

$$\mu = \mu_f + (1-x)\mu_g, \tag{12}$$

where $\mu_f(p)$ and $\mu_g(p)$ are the viscosity of saturated liquid and saturated vapor, respectively, calculated using the model by Fenghour et al. (1998). Also in the two-phase flow scenario, we assume that the transition from laminar to turbulent friction factor occurs at a specific mixture Reynolds number, i.e., $Re = 2100$.

The specific heat flux q on the r.h.s. of the energy balance Eq. (3) accounts for the specific heat flux exchanged between the fluid and its surroundings and is estimated as

$$q = -\pi D U (T - T_0), \tag{13}$$

where U is the heat-transfer coefficient for the pipelines, T is the fluid temperature, and T_0 is the ambient temperature.

2.4. Numerical solution

The governing equations described above can be solved numerically. Specifically, when carbon dioxide is at single-phase flow conditions, the HEM consists of five equations, Eqs. (1)–(3) and (4)–(5), while at two-phase liquid–vapor conditions in three equations, Eqs. (2), (9), and (10). In both cases, the model is written as a system of nonlinear first-order differential equations in the form

$$\boldsymbol{A}\frac{d\boldsymbol{y}}{dz} = \boldsymbol{B}, \tag{14}$$

where the variable vector is $\boldsymbol{y} = [\rho, u, p, h, T]^T$ for single phase flow and $\boldsymbol{y} = [x, p, u]^T$ for two phase flow conditions, respectively. The analytical expressions of the matrices $\boldsymbol{A}$ and $\boldsymbol{B}$ are given in Appendix B. We conveniently recast Eq. (14) as

$$\frac{d\boldsymbol{y}}{dz} = \boldsymbol{A}^{-1}\boldsymbol{B}, \tag{15}$$

and, then, integrated it numerically using the solver *ode45* of Matlab starting from the conditions at the pipe inlet $\boldsymbol{y}(0) = [\rho_0, u_0, p_0, h_0, T_0]^T$ and $\boldsymbol{y}(0) = [x_0, p_0, u_0]^T$, respectively.

Table 1
Parameters defining the scenario of analysis inspired by the Cortez pipeline.

Parameter	Value/PDFs
L (km)	800
D (mm)	762
β (rad)	0
U (W/m^{2}K)	1
T_{amb} (°C)	5, 20, 35
p_0 (MPa)	$\mathcal{U}(7.5, 20)$, $\mathcal{N}(11, 1.1)$
T_0 (°C)	$\mathcal{U}(0, 30)$, $\mathcal{N}(25, 2.5)$
u_0 (m/s)	$\mathcal{U}(2, 4)$, $\mathcal{N}(2.25, 2.25\text{E}-01)$

The transition between the single-phase and the two-phase model is handled by discretizing the pipe domain (of length L) in N equal elements of equal size $\Delta z = L/N$ and checking at each discrete position whether the solution crosses the saturation conditions. When the solution meets the saturation condition from the liquid region, namely from above the saturation line in the $p-T$ diagram, the next cell is initialized as a two-phase state, and the vapor title is set to zero. Instead, when the solution meets the saturation condition from the gas region, the next cell is initialized as a two-phase state, and the vapor title is set to one. To capture more precisely the spatial location where the transition between single and two-phase flow conditions happens, a local grid refinement is adopted in proximity to the transition. An analogous procedure on the vapor title has been implemented to capture the transition from a two-phase to a single-phase state: if x reaches zero the trajectory exits the saturation dome towards the liquid region while if x reaches one it exits towards the gas region. Furthermore, the solution is limited to single-phase liquid, vapor, supercritical, and only liquid–vapor two-phase states, and the transition towards gas/solid states is prevented (i.e., the model cannot go beyond the triple point).

3. Material and methods

3.1. Scenario

As a practical scenario, we consider the Cortez pipeline which supplies CO_2 from the McElmo Dome (Colorado, USA) to Denver crossing the Rocky Mountains (Metz et al., 2005). This is 803 km long with an internal diameter of 762 mm, built in 1982 with an estimated capacity of 20 Mt CO_2 per year (Oosterkamp and Ramsen, 2008). In our study, we consider the typical conditions for carbon dioxide transport in pressurized pipelines (Oosterkamp and Ramsen, 2008; Li et al., 2011; Peletiri et al., 2018) and the available data on the Cortez pipeline. The typical operating pressure is in the range 7.5–20 MPa and should be sufficiently high to guarantee that carbon dioxide is in a dense liquid or supercritical state to avoid two-phase flow conditions. The operating window for temperature, instead, is constrained by the industrial processes of carbon sequestration and the ambient temperature, typically in the range 273.5 to 303.15 K (Li et al., 2011). The overall heat transfer coefficient has been chosen accordingly to similar applications in the literature where it ranges from 0.5 to 5 W/m^{2}K (Lu and Connell, 2008; Brown et al., 2015); in this work the parameter is chosen equal to the unity as listed in Table 1. The pipeline is assumed to be horizontal and, therefore, the pipe inclination is set to $\beta = 0$.

3.2. Stochastic framework

The quantities of interest (QoIs) which we evaluate with the model are: (i) the velocity $u(z)$, (ii) the pressure $p(z)$, (iii) the temperature $T(z)$, (iv) the location where the transition from single-phase to two-phase condition takes place z_{tp}, and (v) the location where the carbon dioxide reaches the triple point (namely, ice start to form into the pipeline) z_f. These are used to measure the effect of the inlet conditions

(p_0, T_0, u_0) on the efficiency and safety of transporting carbon dioxide in a pressurized pipeline. Specifically, z_{tp} gives information about the necessity (or not) of repressurization along the pipeline while z_{f} clearly identifies conditions where the pipeline may fail due to freezing.

In this work, we set the pipeline length, L, diameter, D, capacity, the heat transfer coefficient U, and the pipe inclination β while we continuously span the QoIs over their range of variation given by the boundary conditions at the inlet, i.e. p_0, T_0, and u_0. Doing so, our analysis is mimicking the operation conditions by modeling the boundary conditions as random variables. Specifically, we conduct two different analyses. In the first one, we focus on z_{tp} and z_{f}, and we consider a uniform distribution for the three parameters to perform Global Sensitivity Analysis (GSA) and map z_{tp} and z_{f} on a wide range of realistic operating conditions. In the second one, we consider a variability at the inlet around the average operating condition for the Cortez pipeline, i.e. p_0, T_0, and u_0 are represented as normal random variables, in this case, with a coefficient of variation equal to 0.1, to compute the moments of the flow features, $u(z)$, $p(z)$, and $T(z)$. The parameters defining the scenario we are analyzing are collected in Table 1. The main idea is to explore the parameter space deriving surrogates (as reported in the next Section) without relying on computationally expensive Monte Carlo simulations on the numerical model.

3.3. Polynomial Chaos Expansion

Here, we introduce the Polynomial Chaos Expansion (PCE) theory. The goal is to derive surrogates that express the QoIs as functions of selected parameters. Each surrogate enables reconstructing continuously the response surface for the corresponding QoI in the parameter space with a quite limited computational cost.

We define with $\Omega = f(\mathbf{p})$, with $\dim(\mathbf{p}) = M$, a QoI, depending on a selected subset of M parameters, computed through the high-fidelity model (HFM) f. If $\sigma_\Omega^2 < \infty$, the PCE approximation holds and reads as follows (Xiu and Karniadakis, 2002)

$$\hat{\Omega} = \sum_{\mathbf{a}\in\mathbb{N}^M} s_{\mathbf{a}} \Psi_{\mathbf{a}}(\mathbf{p}), \tag{16}$$

where $\mathbf{a} = \{a_1, \dots, a_M\} \in \mathbb{N}^M$ are multi-indices associated with the multivariate polynomials $\Psi_{\mathbf{a}}$ of degree $|\mathbf{a}| = \sum_{i=1}^{M} a_i$. The polynomials represent an orthonormal basis with respect to the joint PDF of the parameters (Xiu and Karniadakis, 2002), while the $s_{\mathbf{a}}$ are the deterministic coefficients of the expansion. The PCE is conveniently truncated at a maximum degree q as

$$\hat{\Omega} = \sum_{i=0}^{P-1} s_i \Psi_i(\mathbf{p}), \qquad P = \frac{(M+q)!}{M!q!}, \tag{17}$$

i.e., $|\mathbf{a}| \le q$ for all $\mathbf{a} \in \mathbb{N}^M$.

The polynomial basis is selected according to the generalized PCE theory introduced by Xiu and Karniadakis (2002), while the coefficients are computed with a regression method. Specifically, σ_ε^2 is minimized with respect to the coefficients, where $\varepsilon = |\hat{\Omega} - \Omega|$ is the residual given by the difference between the QoI computed with the HFM and PCE respectively (e.g. Ciriello et al., 2017).

In our study, we select as QoIs $u(z), p(z), T(z), z_{\text{tp}}, z_{\text{f}}$, and p_0, T_0, u_0 as governing parameters, i.e., $M = 3$. By employing a second-order PCE, the number of regression points is 10 (e.g. Ciriello et al., 2017), which corresponds to the number of runs of the HFM necessary to perform the regression and compute the PCE coefficients against the case study. This number substitutes the number of MC simulations, at least two orders higher, required for uncertainty quantification analyses directly on the HFM. Once the PCE surrogate is available, these analyses are associated with a negligible computational cost (Ciriello et al., 2017).

In particular, a Global Sensitivity Analysis (GSA) (Sobol', 2001) can be performed through a simple analytical post-processing of the PCE coefficients, avoiding onerous MC simulations of the HFM (e.g. Ciriello et al., 2017). We compute the Sobol indices, where each principle sensitivity index, S_i, is given by

$$S_i = \frac{\sum_{\gamma\in\Gamma_i} s_\gamma^2 \left\langle \Psi_\gamma^2(p_i) \right\rangle}{\sigma_\Omega^2}, \qquad \sigma_\Omega^2 = \sum_{i=1}^{P-1} s_i^2 \left\langle \Psi_i^2(\mathbf{p}) \right\rangle \tag{18}$$

where $\Gamma_i = \{\gamma \in (1, \dots, P-1) : \Psi_\gamma(p_i)\}$. Here, S_i quantify the influence of the parameter p_i on the model variance of Ω, i.e. σ_Ω^2, as (Sudret, 2008). In addition to that, the total sensitivity index, ST_i, sums the principal sensitivity index of the parameter with the indices that express the influence of that parameter with the others (Sobol', 2001). As such, if S_i represents the reduction in σ_Ω^2 if p_i is not uncertain, ST_i, quantifies the residual σ_Ω^2 if only p_i is uncertain (Sobol', 2001).

4. Results and discussion

4.1. High-fidelity simulations

In this Section, we present a set of simulations of the steady-state transport of carbon dioxide obtained with the high-fidelity model. In Fig. 1, we present the trajectories of the main thermodynamic variables for three simulations conducted under representative operational conditions in the selected operational window for p_0 and T_0 defined in Section 3.1. Simulation 1 features high inlet temperature and pressure, set at $p_0 = 20$ MPa, $T_0 = 30$ °C. Simulation 2 has intermediate inlet pressure and temperature, with $p_0 = 15$ MPa, $T_0 = 15$ °C. Finally, simulation 3 is characterized by low inlet temperature and pressure, with $p_0 = 7.5$ MPa, $T_0 = 0$ °C. In all three scenarios, the velocity is maintained at an intermediate value, $u_0 = 3$ m/s, and the ambient temperature is $T_{\text{amb}} = 20$ °C.

At the inlet, the carbon dioxide is in a dense liquid single-phase state (Fig. 2(a)), and, due to the friction between the fluid and the pipe wall, the pressure decreases along the axial direction (see Fig. 1(b)). Interestingly, the temperature also decreases along the pipeline due to the competition between the heat transfer with the environment and real-gas effects (see Fig. 1(c)). Specifically, although the environment (set at $T_{amb} = 20, °C$) tends to equilibrate with the flow—heating the pipeline in simulations 2 and 3 (where the initial temperatures are 15 and $0, °C$, respectively) and cooling it in simulation 1 (where the initial temperature is $30, °C$)—we observe a temperature decrease in all three cases. This can be explained by noting that real-gas effects dominate over heat transfer with the environment. In fact, real-gas effects can be quantified by the Joule–Thompson coefficient $\mu_{JT} = (\partial T/\partial p)_h$, namely the ratio of the temperature decrease to the pressure drop. In pipe flow, since pressure decreases due to pressure drop, when $\mu_{JT} > 0$ the flow tends to cool down, while for $\mu_{JT} < 0$ the flow heats up. As shown in Fig. 2(b), the Joule–Thompson coefficient is positive within the transport window, and therefore, the carbon dioxide cools down along the pipeline. Indeed, in all simulations, this mechanism dominates over heat transfer from $z = 0$ m to the transition to two-phase flow at z_{tp}.

After a certain distance, z_{tp}, the trajectory meets the saturation line and the flow switches to two-phase flow conditions. This transition is undesirable during transport because the flow cools down rapidly (the Joule–Thompson coefficient of two-phase states is positive due to the Clausius–Clapeyron relation, (Gyftopoulos and Beretta, 2005)), and both pressure and temperature drop to the triple point conditions ($p_{\text{tp}} = 517$ kPa, $T_{\text{tp}} = 216.55$ K). As a result, the density decreases by approximately an order of magnitude, leading to a decrease in flow speed to conserve mass, which ultimately reduces the transport efficiency in terms of volumetric flux. The location in the pipeline where triple point conditions are reached and where ice begins to form is referred to as the freezing point, z_{f}.

It is clear that we should avoid transitioning to two-phase flow conditions during transport operations. One effective way to achieve this is by adding a repressurization station, which can restore the pressure to a level sufficient to prevent the transition. In the next

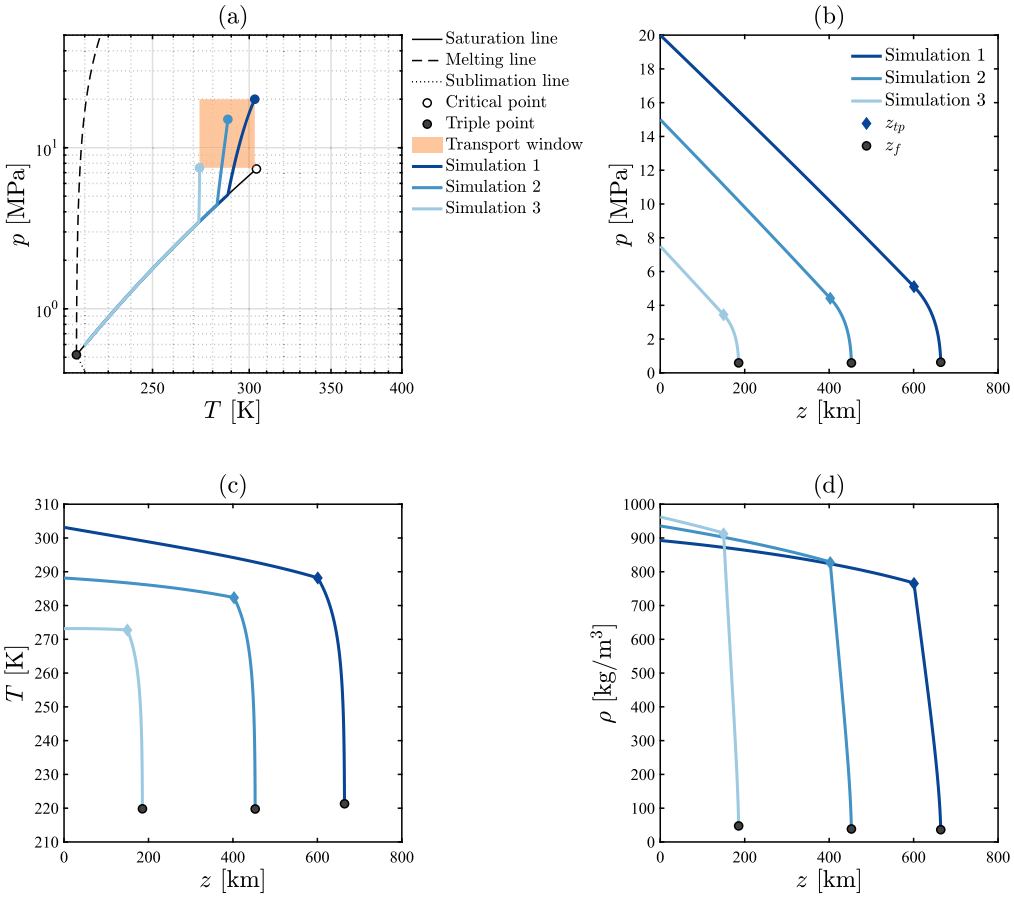

Fig. 1. Evolution of the main thermodynamic variables in three representative high-fidelity simulations in the selected operational transport window. Simulation 1 p_0 = 20 MPa, T_0 = 30 °C, simulation 2 p_0 = 15 MPa, T_0 = 15 °C, simulation 3 p_0 = 7.5 MPa, T_0 = 0 °C. In all three scenarios, u_0 = 3 m/s, and T_{amb} = 20 °C. Specifically, panels show (a) the $p-T$ diagram, (b)–(d) the evolution of p, T, and ρ as a function of the axial coordinate z, respectively.

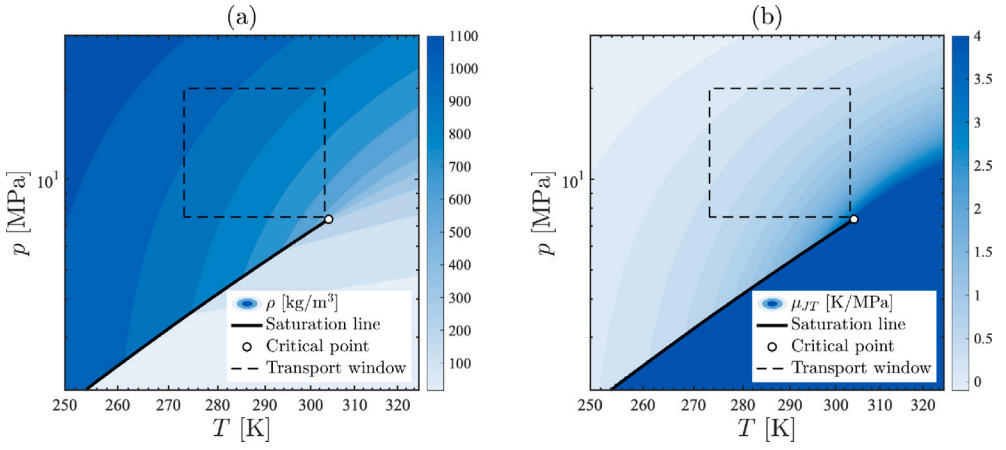

Fig. 2. (a) Density of carbon dioxide, ρ, in the $p-T$ diagram; (b) Joule–Thompson coefficient, μ_{JT}, of carbon dioxide in the $p-T$ diagram.

section, we will discuss how the distance z_{tp} is affected by the inlet parameters to identify optimal operational conditions to avoid two-phase flows. We will extend the analysis to the freezing point distance to be intended for the conditions where the carbon dioxide freezes inside the pipeline (Pham and Rusli, 2016).

4.2. Analysis of two-phase and freezing conditions

In this Section, we aim to provide an exhaustive understanding of the effect of the variability of the inlet conditions, mimicking the operation conditions, on the maximal distance before a repressurization is needed, and the maximal distance before the carbon dioxide will start freezing inside the pipeline. Our goal is to provide a map of z_{tp} and z_f in the (p_0, T_0, u_0) space of variability as a basis for risk quantification, and the definition of optimal design and operation conditions. As before, we refer to the operational windows for the inlet pressure, velocity, and temperature typical of carbon dioxide transport defined in Section 3.1.

To reconstruct the value of the QoIs in the operational windows, we use PCE-based surrogates as explained in Section 3.3. Specifically, we derived two 2nd-order PCEs to approximate $z_{tp}(p_0, T_0, u_0)$

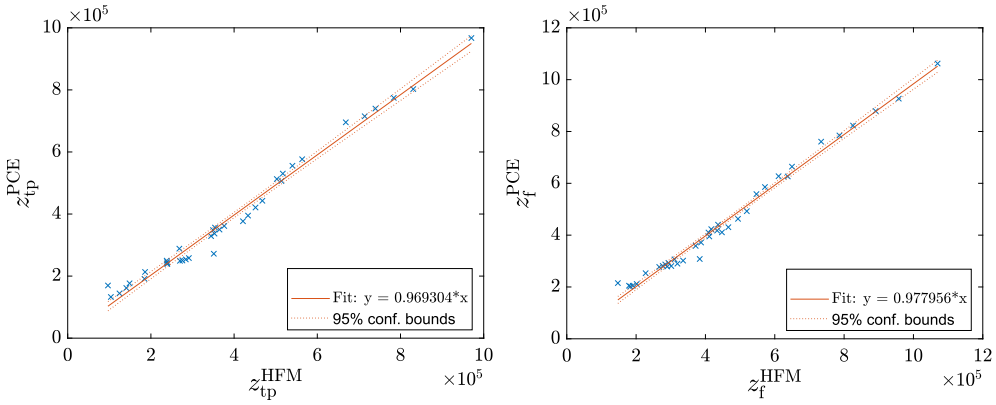

Fig. 3. Validation of the 2nd-order PCE surrogates for the QoIs z_{tp} (m), and z_f (m) at T_{amb}=20 °C.

Table 2
Sensitivity Indices of Sobol for z_{tp} and z_f at T_{amb}=20 °C. ST_i is the total sensitivity index, S_i is the principal sensitivity index, and $ST_{i,j}$ is the second-order sensitivity index, respectively.

	z_{tp}	z_f
ST_{u_0}	0.590	0.665
ST_{T_0}	0.008	0.018
ST_{p_0}	0.519	0.410
S_{u_0}	0.477	0.573
S_{T_0}	0.002	0.012
S_{p_0}	0.404	0.322
S_{u_0,T_0}	0.002	0.004
S_{u_0,p_0}	0.111	0.087
S_{T_0,p_0}	0.004	0.002

and $z_f(p_0, T_0, u_0)$. A 2nd-order approximation is sufficient to properly describe these QoIs as shown in Fig. 3 where we validate the predictions of the surrogates against a set of Monte Carlo simulations obtained solving the HEM. The validation denotes a high level of accuracy of both approximations. Note that this level of accuracy is achieved using only 10 high-fidelity simulations to calibrate the surrogates. Then, once the surrogates are available, we can easily span the entire space of variability for the parameters.

We then compute the Sobol indices for the two QoIs, as collected in Table 2. The principal sensitivity indices, S_i, establish the priority among inputs to reduce output variance, while total sensitivity indices, ST_i, measure the overall effect of each input on the output variance. As such, they discriminate which inputs do not significantly influence the response and can be treated as single-point values to reduce the problem's dimensionality. The overall trend of the sensitivity indices is quite similar for both z_{tp} and z_f. Specifically, referring to the detailed GSA to T_{amb} = 20 °C, the model variance is primarily affected by the inlet pressure and velocity, while the impact of the inlet temperature T_0 is negligible. Thus, within the operational window for transport of CO_2 in pipelines (i.e., 7.5 – 20 MPa and 273.5 to 303.15 K), the maximal distance before a repressurization is needed to avoid two-phase flow conditions can be determined looking at the inlet pressure and velocity only.

Interestingly, the fact that the variance of z_{tp} is primarily affected only by the variability of u_0 and p_0 (see Table 2) is not straightforward. This finding is confirmed by the HEM simulations shown in Fig. 4, which illustrate the effect of inlet temperature on the occurrence of two-phase flow for p_0 = 15 MPa. Although we might intuitively expect T_0 to have an influence by affecting the fluid's material properties, Fig. 4(b) clearly shows that the slope of the pressure drop is only slightly affected by the inlet temperature. In the operational window, in fact, carbon dioxide remains in a dense liquid state, and its material properties are primarily a function of pressure. The joint impact of u_0 and p_0 affects the variance of the two QoIs, as indicated by the second-order Sobol index in Table 2, $ST_{i,j}$ as a minor effect. The entire variance of z_{tp} is evenly determined by u_0 and p_0, while u_0 is the most influential parameter for the prediction of z_f.

These results do not fundamentally change if we vary the ambient temperature to describe more extreme scenarios as cold and hot environments. Specifically, we compute and compare the total sensitivity indices for different values of T_{amb} = 5, 20, 35 °C (Fig. 5). While obtaining a negligible effect of T_0 also in case of extreme external temperatures, we observe that the overall impact of u_0 decreases when T_{amb} increases, in favor of p_0, especially in case of z_{tp}, for which the respective total sensitivity indices get almost the same value when T_{amb} = 35 °C. This can be explained by the fact that real-gas effects (i.e., the cooling of supercritical carbon dioxide due to the Joule–Thomson effect) dominate over heat transfer with the external environment (see the discussion of the simulations presented in Section 4.1). It is worth noting that we are considering a scenario in which the pipeline is insulated and the overall heat transfer coefficient is quite low (see Table 1). In alternative scenarios where the pipeline is not well insulated, the heat transfer mechanism competes with real-gas effects in the energy equation, and the temperature of the carbon dioxide increases (tending to equilibrate with the environment) instead of decreasing (due to the sign of μ_{JT}), as shown in Fig. 6. This effect becomes more pronounced as U increases and will inevitably also influence the results of the sensitivity analysis.

To offer a deeper insight into the impact of inlet operational choices, in Fig. 7 we provide the map of z_{tp} in the space (T_0, p_0) and (u_0, p_0) for different values of u_0 and T_0 respectively. The idea is to show the contours of the location where the transition to two-phase occurs for the mean and the two extremes of the range of variability considered for u_0 (left) and T_0 (right). In the space (T_0, p_0), we observe that the variability of z_{tp} is almost only along the vertical axis, i.e., for varying p_0 as expected from the results of the GSA. In the selected range of operation conditions, z_{tp} varies notably from about 150 to 550 km for u_0 = 3 m/s, revealing the impact of p_0 on the location at which the transition from single-phase to two-phase condition occurs. For u_0 = 2 m/s, we observe a similar behavior of z_{tp} in (T_0, p_0) but it varies from about 300 to 1100 km. Differently, when u_0 = 4 m/s, the map of z_{tp} in (T_0, p_0) exhibits a more complex nonlinear behavior also along T_0, but the range of variability reduces to about 150 to 240 km in this case. In the space (u_0, p_0), we observe that z_{tp} increases as p_0 increases and u_0 decreases, indicating the influence of both parameters. This trend is consistent across different values of T_0, with z_{tp} varying, in all cases, within a range of approximately 200 to 1000 km.

As for the pipeline's section where the carbon dioxide reaches the triple point, z_f, map is provided in Fig. 8 in the space (T_0, p_0) and

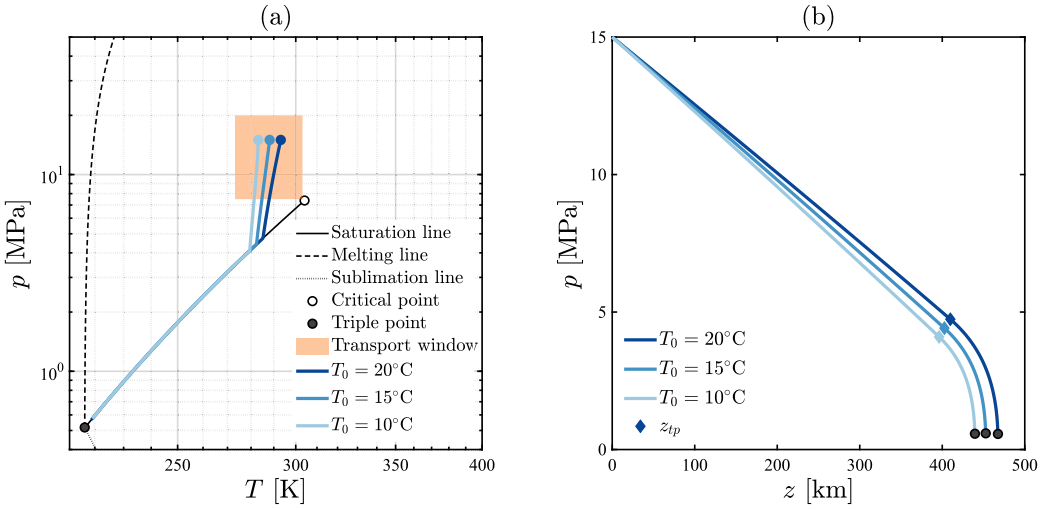

Fig. 4. Effect of the inlet temperature on the occurrence of two-phase flows for $p_0 = 15$ MPa and $T_0 = 20$ °C, $T_0 = 15$ °C, $T_0 = 10$ °C. In all three cases, $u_0 = 3$ m/s, and $T_{amb} = 20$ °C.

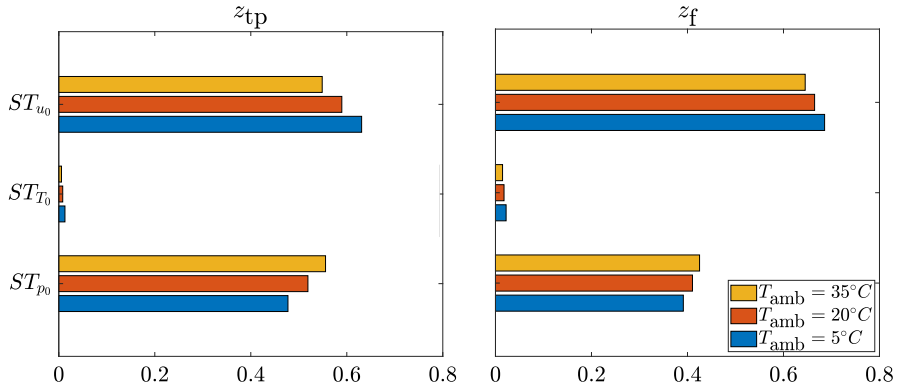

Fig. 5. Total Sensitivity Indices of Sobol for z_{tp} and z_f for different values of T_{amb}.

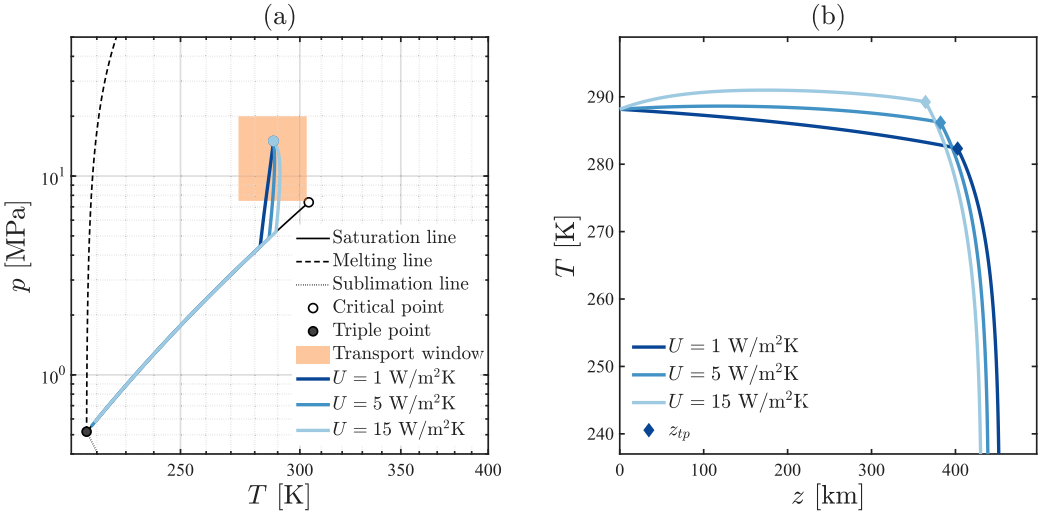

Fig. 6. Effect of the overall heat-transfer coefficient U on the occurrence of two-phase flows for $p_0 = 15$ MPa and $T_0 = 20$ °C. In all three cases, $u_0 = 3$ m/s, and $T_{amb} = 20$ °C.

(u_0, p_0) for different values of u_0 and T_0 respectively. We observe a notably equivalent behavior as z_{tp} with slightly higher values for z_f. Overall, these maps provide insightful information to design appropriate operation conditions to minimize the risk of undesirable events and the cost associated with repressurization stations. Indeed, following our approach, it is possible to identify the field of operation condition for a given plant, that maximizes the distance at which repressurization is needed. This corresponds to high p_0 and low u_0 for any T_0 in the operational window considered.

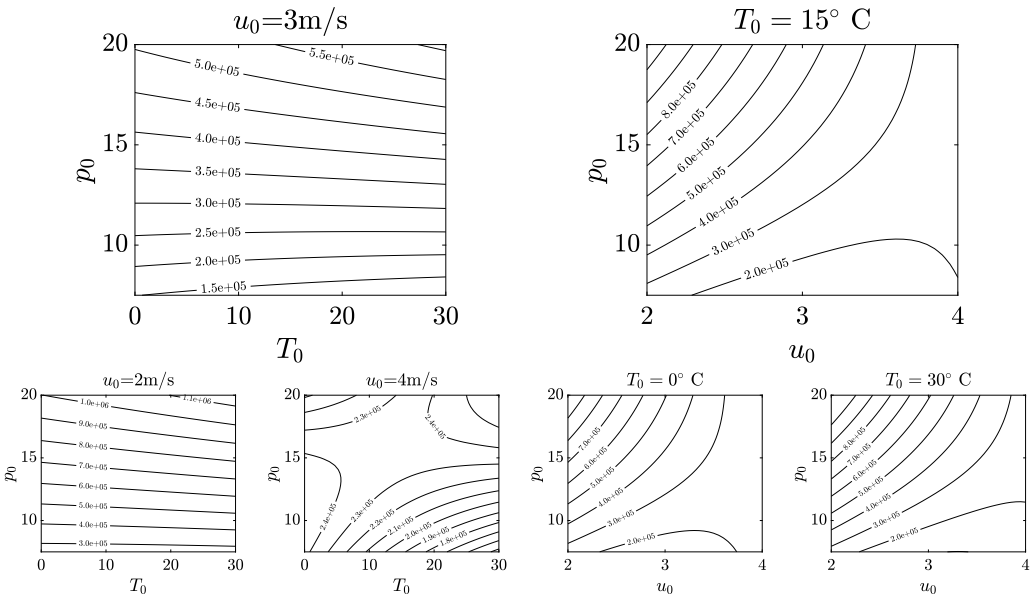

Fig. 7. Mapping of the surface of z_{tp} (m) for T_{amb}=20 °C.

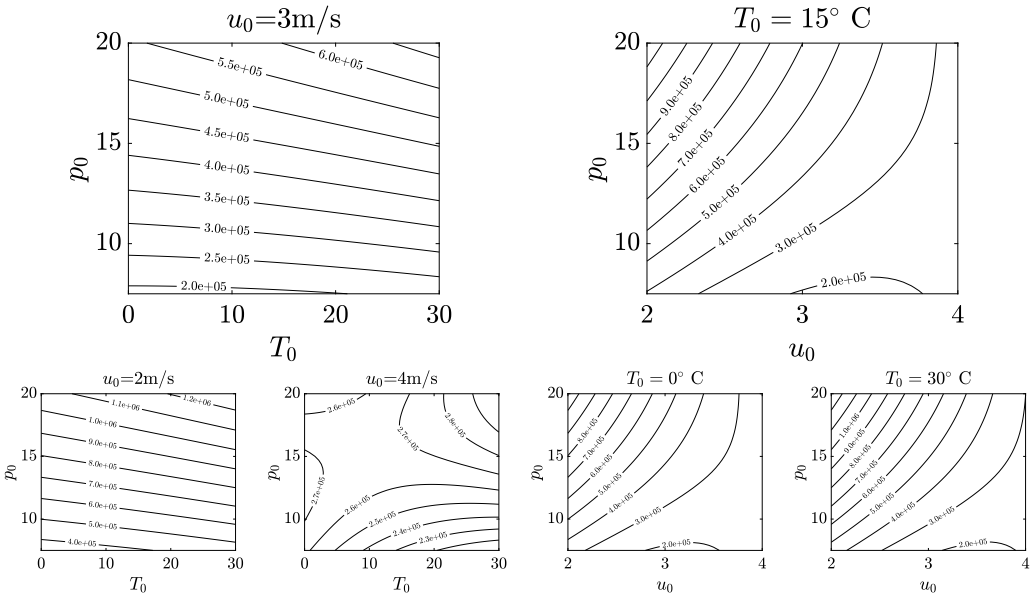

Fig. 8. Mapping of the surface of z_f (m) for T_{amb}=20 °C.

4.3. Analysis of flow characteristics under uncertainty

In this Section, the main idea is to study how the uncertainty of a specific design condition (i.e., the value for T_0, p_0, and u_0 is picked up from a probability distribution function centered in the design condition) affects the model outputs (i.e., the flow characteristics). To do so, we examine the average operating conditions at the inlet associated with the Cortez pipeline, i.e., p_0 = 11 MPa, u_0 = 2.25 m/s, T_0 = 25 °C, and introduce uncertainty into the scenario using a coefficient of variation of 0.1 for all three parameters (see Table 1). We then compute via PCE the statistical moments for $u(z)$, $T(z)$, and $p(z)$, i.e., the mean $\overline{u}(z)$, $\overline{T}(z)$, and $\overline{p}(z)$ and the variance $V_u(z)$, $V_T(z)$, and $V_p(z)$.

The present analysis is limited to the typical operational conditions for pressure and temperature outlined in Section 3.1. Specifically, the operating pressure is within the optimal range shown in Fig. 9, and, therefore, we limit our analysis to a length of 300 km, where the pressure remains, on average, above 7.5 MPa. Hence, the simulations are rather below the transition to two-phase flow conditions z_{tp} that is, based on the results obtained in the previous Section, between 400 and 500 km (Fig. 7).

In the first column of Fig. 9, the mean of the three QoIs along the pipeline is represented with a confidence level of ± one standard deviation. The mean of pressure and temperature decreases almost linearly along z, while the mean of the velocity slightly increases. Interestingly, the uncertainty analysis provides information on the statistical moments for the pressure at a specific location. That equips the confidence level in predictions for the HEM so that we can quantify the uncertainty of pressure drop predictions due to the variability of the input parameters. In fact, despite the HEM being widely used in research and for real-time control strategies, the propagation of input uncertainties in predictions has not been deeply investigated in the literature. In our case study, we observe that the standard deviation increases for the pressure along the pipeline from about 1.10 to 1.20 MPa, which brings the coefficient of variation from 0.10 to 0.17, thus

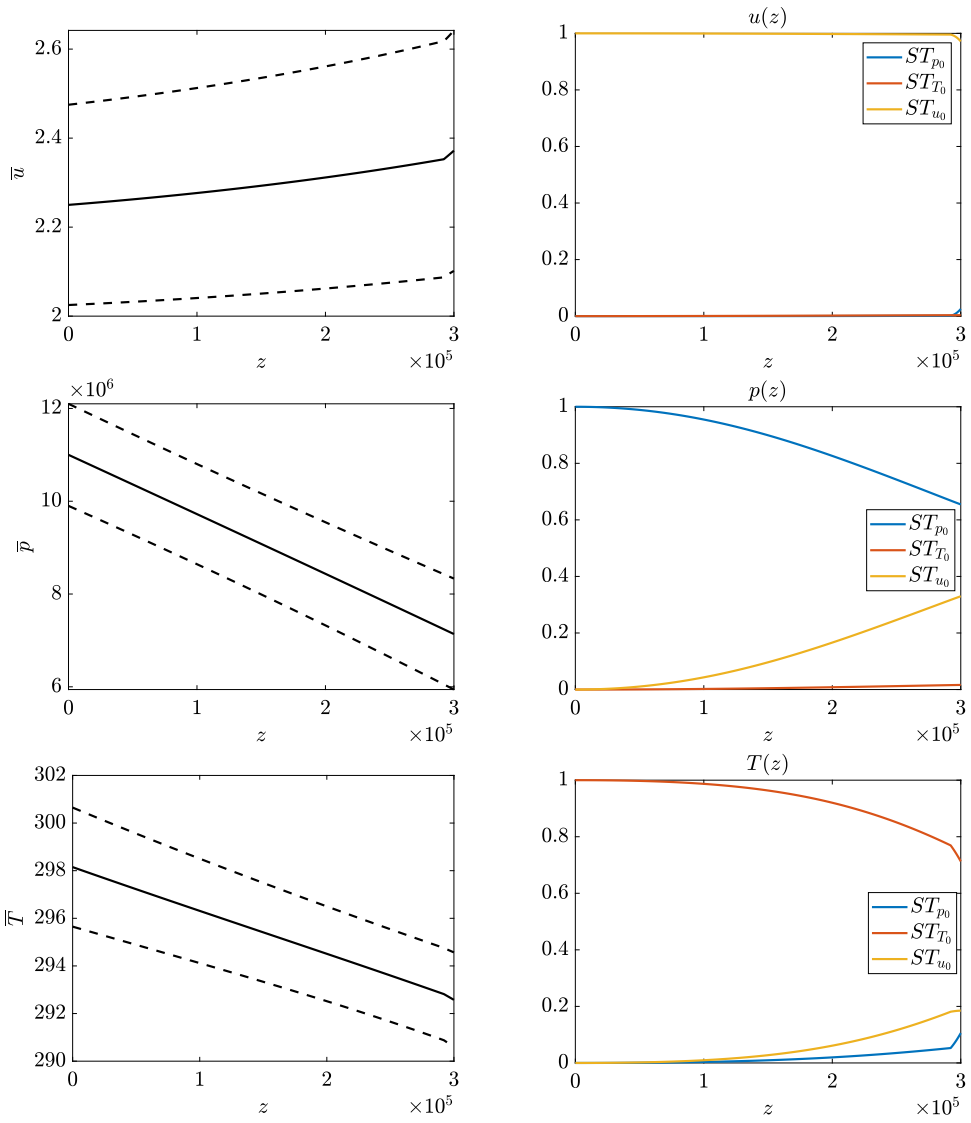

Fig. 9. Mean of the QoIs $u(z)$ (m/s), $p(z)$ (Pa), and $T(z)$ (°C), with a confidence level of ± one standard deviation (first column), and total sensitivity indices for the same QoIs associated with the inlet parameters (second column).

denoting the impact of the variability in inlet parameters even if limited around a design operating condition. Less relevant, for the temperature and the velocity along the pipeline, the coefficient of variation goes from 8.4E−03 to 6.82E−03 and from 0.10 to 0.11, respectively.

We also repeated the GSA for $u(z)$, $T(z)$, and $p(z)$ by computing the total sensitivity indices along the pipeline associated with the inlet parameters, as shown in the second column of Fig. 9. While the variance in the velocity is exclusively due to the variability in u_0, the variance of the pressure is explained by both the variability in p_0 and u_0, with the latter becoming more influent, at expenses of p_0, as z increases. When considering the variance in the temperature, T_0 governs it, but its importance decreases due to the pressure drop in favor of the other two inlet parameters.

5. Conclusions

In this study, we analyze the steady-state transport of carbon dioxide in pipelines, emphasizing the critical role of operational parameters in avoiding two-phase flow and freezing conditions. We show that the Homogeneous Equilibrium Model can be effectively combined with a polynomial-chaos-based surrogate, allowing uncertainty and sensitivity analyses to be performed at minimal computational cost. Our findings indicate that the inlet pressure and velocity are the most influential parameters in determining the maximal distance before a repressurization is needed to avoid transitioning to a two-phase flow. This conclusion is supported by a global sensitivity analysis, which shows that the inlet temperature has a negligible impact on these outcomes within the operational window of interest. Using high-fidelity simulations and PCE-based surrogates has proven effective in modeling the system under uncertainty. The surrogates enable the exploration of the entire parameter space efficiently and accurately even with limited high-fidelity simulations. The validation against Monte Carlo simulations demonstrates that the 2nd-order PCEs are highly accurate, offering a reliable tool for sensitivity analysis and design optimization. Indeed, the mapping of the transition point and freezing point distances in the operational space provides crucial information for pipeline design. It allows operators to optimize the transport conditions by selecting the appropriate pressure and velocity combinations, thereby minimizing the risk of undesirable events. Finally, once specific operation conditions are selected, we show how in the same methodological framework, it is possible to accommodate uncertainty quantification to equip the prediction of flow characteristics with the proper level of confidence, through the computation of the statistical moments along the pipeline. In conclusion, the approach developed in this study

provides a comprehensive understanding of the impact of operational parameters on the transport of carbon dioxide in pipelines and the method is easily adaptable to various plant scenarios including a larger set of key governing parameters. We finally recall that the current study is focused on presenting the new theoretical framework which combines the HEM with the PCEs and the results cover the case of pure carbon dioxide only for the sake of simplicity. In future works we aim at extending extend the framework to more realistic scenarios, for example including the effect of impurities and transient dynamics.

CRediT authorship contribution statement

Davide Picchi: Writing – review & editing, Writing – original draft, Methodology, Funding acquisition, Formal analysis, Conceptualization. **Valentina Ciriello:** Writing – review & editing, Writing – original draft, Methodology, Funding acquisition, Formal analysis, Conceptualization.

Declaration of competing interest

The authors declare that they have no known competing financial interests or personal relationships that could have appeared to influence the work reported in this paper.

Acknowledgments

This study has received funding from the European Union "NextGenerationEU", Ministero dell'Università e della Ricerca (MUR) "Italiadomani" Piano Nazionale di Ripresa e Resilienza (PNRR), Mission 4, Research Project PRIN 2022 "Predictive forecasting and risk assessment for CO2 transport in pipelines", MUR code: 20229JPN53; CUP code: J53D2300200 0006 CUP code: D53D23003250006.

Appendix A. Peng–Robinson equation of state (EoS)

The Peng and Robinson (1976) equation of state reads:

$$p = \frac{RT}{v-b} - \frac{a}{v(v+b)+b(v-b)}, \tag{A.1}$$

where

$$a = 0.45724\frac{R^2T_c^2}{p_c}\alpha \qquad b = 0.07780\frac{RT_c}{p_c}, \tag{A.2}$$

$$\alpha = (1+m(1-\sqrt{T_r}))^2, \tag{A.3}$$

$$m = 0.37464 + 1.54226\omega - 0.26992\omega^2, \tag{A.4}$$

with ω the acentric factor, $T_r = T/T_c$ the reduced temperature, and R the gas constant. For the case of carbon dioxide, $\omega = 0.225$ and $R = \mathcal{R}/M_m = 188.91$ J/kgK (the universal gas constant $\mathcal{R} = 8.314$ kJ/kmolK and the molecular weight $M_m = 44.01$ kg/kmol).

The HEM introduced in Section 2 requires a consistent model for the specific heat capacity at constant pressure c_p, the isobaric expansion coefficient α_p, and the isothermal compressibility coefficient κ_T. Given the EoS Eq. (A.1), $c_p(T,p) = (\partial h/\partial T)_p$ can be easily computed starting from the departure function for the enthalpy and, then, differentiating with respect to the temperature, see Klein and Nellis (2011) and Poling et al. (2001). Manipulating Eq. (A.1) the analytical expressions for the compressibility coefficients can be easily derived as

$$\alpha_p = \frac{1}{v}\left[\frac{\frac{Rv^2}{p} - v\left(\frac{a}{\alpha p}\frac{d\alpha}{dT} - \frac{2Rb}{p}\right) - \frac{Rb^2}{p} + \frac{ab}{\alpha p}\frac{d\alpha}{dT}}{3v^2 + 2v\left(b - \frac{RT}{p}\right) + \frac{a}{p} - 3b^2 - \frac{2RTb}{p}}\right], \tag{A.5}$$

$$\kappa_T = -\frac{1}{v}\left[\frac{-RT(v^2+2bv-b^2)^2 + a(2v+2b)(v-b)^2}{(v-b)^2(v^2+2bv-b^2)^2}\right]^{-1} \tag{A.6}$$

where

$$\frac{d\alpha}{dT} = -\frac{m\sqrt{\alpha}}{T_c\sqrt{T_r}}. \tag{A.7}$$

Appendix B. HEM in matrix form

For single phase flow conditions the variable vector is $\boldsymbol{y} = [\rho, u, p, h, T]^T$ and the model matrices reads

$$\boldsymbol{A} = \begin{bmatrix} u & \rho & 0 & 0 & 0 \\ 0 & \rho u & 1 & 0 & 0 \\ 0 & u & 0 & 1 & 0 \\ -\frac{1}{k_T\rho} & 0 & 1 & 0 & -\frac{\alpha_p}{k_T} \\ 0 & 0 & (1-T\alpha_p)v & -1 & c_p \end{bmatrix}, \tag{B.1}$$

$$\boldsymbol{B} = \begin{bmatrix} 0 & -\frac{f\rho u^2}{2}\frac{S}{A} + \rho g\sin(\theta) & -\frac{qS}{uA\rho} + g\sin(\theta) & 0 & 0 \end{bmatrix}^T. \tag{B.2}$$

For two-phase flow conditions the variable vector is $\boldsymbol{y} = [x, p, u]^T$ and the model matrices reads

$$\boldsymbol{A} = \begin{bmatrix} -\frac{u}{v^2}\left(\frac{dv_f}{dp} + x\frac{dv_{fg}}{dp}\right) & -\frac{uv_{fg}}{v^2} & \frac{1}{v} \\ 1 & 0 & \frac{u}{v} \\ \frac{dh_f}{dp} + x\frac{dh_{fg}}{dp} & h_{fg} & u \end{bmatrix} \tag{B.3}$$

$$\boldsymbol{B} = \begin{bmatrix} 0 & -\frac{f\rho u^2}{2}\frac{S}{A} + \rho g\sin(\theta) & -\frac{qS}{uA\rho} + g\sin(\theta) \end{bmatrix}^T. \tag{B.4}$$

Data availability

Data will be made available on request.

References

Abedini, A., Torabi, F., 2014. On the CO2 storage potential of cyclic CO2 injection process for enhanced oil recovery. Fuel 124, 14–27. http://dx.doi.org/10.1016/j.fuel.2014.01.084, URL https://www.sciencedirect.com/science/article/pii/S0016236114001033.

Andreussi, P., Persen, L., 1987. Stratified gas-liquid flow in downwardly inclined pipes. Int. J. Multiph. Flow 13 (4), 565–575. http://dx.doi.org/10.1016/0301-9322(87)90022-X, URL https://www.sciencedirect.com/science/article/pii/030193228790022X.

Andritsos, N., Hanratty, T.J., 1987. Influence of interfacial waves in stratified gas-liquid flows. AIChE J. 33 (3), 444–454. http://dx.doi.org/10.1002/aic.690330310, arXiv:https://aiche.onlinelibrary.wiley.com/doi/pdf/10.1002/aic.690330310, URL https://aiche.onlinelibrary.wiley.com/doi/abs/10.1002/aic.690330310.

Angeli, P., Hewitt, G., 1999. Pressure gradient in horizontal liquid–liquid flows. Int. J. Multiph. Flow 24 (7), 1183–1203. http://dx.doi.org/10.1016/S0301-9322(98)00006-8, URL https://www.sciencedirect.com/science/article/pii/S0301932298000068.

Angielczyk, W., Bartosiewicz, Y., Butrymowicz, D., 2020. Development of delayed equilibrium model for CO2 convergent-divergent nozzle transonic flashing flow. Int. J. Multiph. Flow 131, 103351. http://dx.doi.org/10.1016/j.ijmultiphaseflow.2020.103351.

Aursand, P., Hammer, M., Munkejord, S., Wilhelmsen, Ø., 2013. Pipeline transport of CO2 mixtures: Models for transient simulation. Int. J. Greenh. Gas Control. 15, 174–185. http://dx.doi.org/10.1016/j.ijggc.2013.02.012.

Bamidele, O.E., Hassan, M., Ahmed, W.H., 2021. Flow induced vibration of two-phase flow passing through orifices under slug pattern conditions. J. Fluids Struct. 101, 103209. http://dx.doi.org/10.1016/j.jfluidstructs.2020.103209, URL https://www.sciencedirect.com/science/article/pii/S0889974620306782.

Barnea, D., 1987. A unified model for predicting flow-pattern transitions for the whole range of pipe inclinations. Int. J. Multiph. Flow 13 (1), 1–12. http://dx.doi.org/10.1016/0301-9322(87)90002-4, URL https://www.sciencedirect.com/science/article/pii/0301932287900024.

Bendiksen, K., Espedal, M., 1992. Onset of slugging in horizontal gas-liquid pipe flow. Int. J. Multiph. Flow 18 (2), 237–247. http://dx.doi.org/10.1016/0301-9322(92)90086-V, URL https://www.sciencedirect.com/science/article/pii/030193229290086V.

Blasius, H., 1913. Das aehnlichkeitsgesetz bei reibungsvorgängen in flüssigkeiten. In: Mitteilungen Über Forschungsarbeiten Auf Dem Gebiete Des Ingenieurwesens: Insbesondere Aus Den Laboratorien Der Technischen Hochschulen. Springer Berlin Heidelberg, Berlin, Heidelberg, pp. 1–41. http://dx.doi.org/10.1007/978-3-662-02239-9_1.

Blunt, M., Fayers, F., Orr, F.M., 1993. Carbon dioxide in enhanced oil recovery. Energy Convers. Manage. 34 (9), 1197–1204. http://dx.doi.org/10.1016/0196-8904(93)90069-M, URL https://www.sciencedirect.com/science/article/pii/019689049390069M, Proceedings of the International Energy Agency Carbon Dioxide Disposal Symposium.

Bonzanini, A., Picchi, D., Poesio, P., 2017. Simplified 1D incompressible two-fluid model with artificial diffusion for slug flow capturing in horizontal and nearly horizontal pipes. Energies 10 (9), http://dx.doi.org/10.3390/en10091372, URL https://www.mdpi.com/1996-1073/10/9/1372.

Brauner, N., Ullmann, A., 2004. Modelling of gas entrainment from taylor bubbles. Part a: Slug flow. Int. J. Multiph. Flow 30 (3), 239–272. http://dx.doi.org/10.1016/j.ijmultiphaseflow.2003.11.007, URL https://www.sciencedirect.com/science/article/pii/S0301932203002222.

Brown, S., Mahgerefteh, H., Martynov, S., Sundara, V., Dowell, N.M., 2015. A multi-source flow model for CCS pipeline transportation networks. Int. J. Greenh. Gas Control. 43, 108–114. http://dx.doi.org/10.1016/j.ijggc.2015.10.014, URL https://www.sciencedirect.com/science/article/pii/S1750583615301018.

Brown, S., Martynov, S., Mahgerefteh, H., Chen, S., Zhang, Y., 2014. Modelling the non-equilibrium two-phase flow during depressurisation of CO2 pipelines. Int. J. Greenh. Gas Control. 30, 9–18. http://dx.doi.org/10.1016/j.ijggc.2014.08.013, URL https://www.sciencedirect.com/science/article/pii/S1750583614002394.

Buist, J., Sanderse, B., Dubinkina, S., Henkes, R., Oosterlee, C., 2022. Energy-conserving formulation of the two-fluid model for incompressible two-phase flow in channels and pipes. Comput. & Fluids 244, 105533. http://dx.doi.org/10.1016/j.compfluid.2022.105533.

Buist, J.F.H., Sanderse, B., Dubinkina, S., Oosterlee, C.W., Henkes, R.A.W.M., 2023. Energy-consistent formulation of the pressure-free two-fluid model. Internat. J. Numer. Methods Fluids 95 (5), 869–898. http://dx.doi.org/10.1002/fld.5168, arXiv:https://onlinelibrary.wiley.com/doi/pdf/10.1002/fld.5168, URL https://onlinelibrary.wiley.com/doi/abs/10.1002/fld.5168.

Buist, J., Sanderse, B., Dubinkina, S., Oosterlee, C., Henkes, R., 2024. Energy-stable discretization of the one-dimensional two-fluid model. Int. J. Multiph. Flow 174, 104756. http://dx.doi.org/10.1016/j.ijmultiphaseflow.2024.104756, URL https://www.sciencedirect.com/science/article/pii/S0301932224000375.

Chandel, M.K., Pratson, L.F., Williams, E., 2010. Potential economies of scale in CO2 transport through use of a trunk pipeline. Energy Convers. Manage. 51 (12), 2825–2834. http://dx.doi.org/10.1016/j.enconman.2010.06.020, URL https://www.sciencedirect.com/science/article/pii/S0196890410002323.

Chiofalo, A., Ciriello, V., Tartakovsky, D., 2025. Transfer learning of neural surrogates on multifidelity groundwater simulations. Adv. Water Resour. 206, 105140. http://dx.doi.org/10.1016/j.advwatres.2025.105140.

Cicchitti, A., Lombardi, C., Silvestri, M., Soldaini, G., Zavattarelli, R., 1959. Two-phase cooling experiments: pressure drop, heat transfer and burnout measurements.

Ciriello, V., Lauriola, I., Bonvicini, S., Cozzani, V., Di Federico, V., Tartakovsky, D.M., 2017. Impact of hydrogeological uncertainty on estimation of environmental risks posed by hydrocarbon transportation networks. Water Resour. Res. 53 (11), 8686–8697. http://dx.doi.org/10.1002/2017wr021368.

Ciriello, V., Lauriola, I., Tartakovsky, D.M., 2019. Distribution-based global sensitivity analysis in hydrology. Water Resour. Res. 55 (11), 8708–8720. http://dx.doi.org/10.1029/2019wr025844.

Colebrook, C.F., White, C.M., Taylor, G.I., 1937. Experiments with fluid friction in roughened pipes. Proc. R. Soc. Lond. Ser. A - Math. Phys. Sci. 161 (906), 367–381. http://dx.doi.org/10.1098/rspa.1937.0150.

de Visser, E., Hendriks, C., Barrio, M., Mølnvik, M.J., de Koeijer, G., Liljemark, S., Le Gallo, Y., 2008. Dynamis CO2 quality recommendations. Int. J. Greenh. Gas Control. 2 (4), 478–484. http://dx.doi.org/10.1016/j.ijggc.2008.04.006, TCCS-4: The 4th Trondheim Conference on CO2 Capture, Transport and Storage.

Drew, D.A., 1983. Mathematical modeling of two-phase flow. Annu. Rev. Fluid Mech. 15 (Volume 15, 1983), 261–291. http://dx.doi.org/10.1146/annurev.fl.15.010183.001401, URL https://www.annualreviews.org/content/journals/10.1146/annurev.fl.15.010183.001401.

Dukler, A.E., Wicks, III, M., Cleveland, R.G., 1964. Frictional pressure drop in two-phase flow: A. a comparison of existing correlations for pressure loss and holdup. AIChE J. 10 (1), 38–43. http://dx.doi.org/10.1002/aic.690100117.

Edwards, R.W.J., Celia, M.A., 2018. Infrastructure to enable deployment of carbon capture, utilization, and storage in the United States. Proc. Natl. Acad. Sci. 115 (38), E8815–E8824. http://dx.doi.org/10.1073/pnas.1806504115.

Einstein, A., 1906. Eine neue bestimmung der moleküldimensionen. Ann. Phys., Lpz. 324 (2), 289–306. http://dx.doi.org/10.1002/andp.19063240204.

Fang, Y., Poncet, S., Nesreddine, H., Bartosiewicz, Y., 2019. An open-source density-based solver for two-phase CO2 compressible flows: Verification and validation. Int. J. Refrig. 106, 526–538. http://dx.doi.org/10.1016/j.ijrefrig.2019.05.016, URL https://www.sciencedirect.com/science/article/pii/S0140700719302129.

Fenghour, A., Wakeham, W.A., Vesovic, V., 1998. The viscosity of carbon dioxide. J. Phys. Chem. Ref. Data 27 (1), 31–44. http://dx.doi.org/10.1063/1.556013.

Gyftopoulos, E., Beretta, G., 2005. Thermodynamics: Foundations and applications. In: Dover Civil and Mechanical Engineering, Dover Publications, URL https://books.google.it/books?id=dOYoAwAAQBAJ.

Hammer, M., Morin, A., 2014. A method for simulating two-phase pipe flow with real equations of state. Comput. & Fluids 100, 45–58. http://dx.doi.org/10.1016/j.compfluid.2014.04.030.

Jia, B., Tsau, J.-S., Barati, R., 2019. A review of the current progress of CO2 injection EOR and carbon storage in shale oil reservoirs. Fuel 236, 404–427. http://dx.doi.org/10.1016/j.fuel.2018.08.103, URL https://www.sciencedirect.com/science/article/pii/S001623611831473X.

Klein, S., Nellis, G., 2011. Thermodynamics. Cambridge University Press, http://dx.doi.org/10.1017/CBO9780511994883.

Koornneef, J., Spruijt, M., Molag, M., Ramírez, A., Turkenburg, W., Faaij, A., 2010. Quantitative risk assessment of CO2 transport by pipelines—A review of uncertainties and their impacts. J. Hazard. Mater. 177 (1), 12–27. http://dx.doi.org/10.1016/j.jhazmat.2009.11.068, URL https://www.sciencedirect.com/science/article/pii/S0304389409018664.

Li, H., Jakobsen, J.P., Wilhelmsen, Ø., Yan, J., 2011. PVTxy properties of CO2 mixtures relevant for CO2 capture, transport and storage: Review of available experimental data and theoretical models. Appl. Energy 88 (11), 3567–3579. http://dx.doi.org/10.1016/j.apenergy.2011.03.052.

Lin, S., Kwok, C., Li, R.-Y., Chen, Z.-H., Chen, Z.-Y., 1991. Local frictional pressure drop during vaporization of R-12 through capillary tubes. Int. J. Multiph. Flow 17 (1), 95–102. http://dx.doi.org/10.1016/0301-9322(91)90072-B.

Linga, G., Lund, H., 2016. A two-fluid model for vertical flow applied to CO2 injection wells. Int. J. Greenh. Gas Control. 51, 71–80. http://dx.doi.org/10.1016/j.ijggc.2016.05.009.

Lu, M., Connell, L.D., 2008. Non-isothermal flow of carbon dioxide in injection wells during geological storage. Int. J. Greenh. Gas Control. 2 (2), 248–258. http://dx.doi.org/10.1016/S1750-5836(07)00114-4.

Lu, M., Connell, L.D., 2014. Transient, thermal wellbore flow of multispecies carbon dioxide mixtures with phase transition during geological storage. Int. J. Multiph. Flow 63, 82–92. http://dx.doi.org/10.1016/j.ijmultiphaseflow.2014.04.002, URL https://www.sciencedirect.com/science/article/pii/S0301932214000640.

Mahgerefteh, H., Zhang, P., Brown, S., 2016. Modelling brittle fracture propagation in gas and dense-phase CO2 transportation pipelines. Int. J. Greenh. Gas Control. 46, 39–47. http://dx.doi.org/10.1016/j.ijggc.2015.12.021, URL https://www.sciencedirect.com/science/article/pii/S1750583615301717.

McAdams, W.H., Woods, W.K., Heroman, L.C., 1942. Vaporization inside horizontal tubes, II. Benzene-oil mixture. Trans. ASME 64, 193–200.

Metz, B., Davidson, O., de Coninck, H.C., Loos, M., Meyer, L.A., 2005. IPCC Special Report on Carbon Dioxide Capture and Storage. Prepared by Working Group III of the Intergovernmental Panel on Climate Change. Cambridge University Press, Cambridge, United Kingdom and New York, NY, USA, p. 442.

Munkejord, S.T., Austegard, A., Deng, H., Hammer, M., Stang, H.J., Løvseth, S.W., 2020a. Depressurization of CO2 in a pipe: High-resolution pressure and temperature data and comparison with model predictions. Energy 211, 118560. http://dx.doi.org/10.1016/j.energy.2020.118560.

Munkejord, S.T., Austegard, A., Deng, H., Hammer, M., Stang, H.J., Løvseth, S.W., 2020b. Depressurization of CO2 in a pipe: High-resolution pressure and temperature data and comparison with model predictions. Energy 211, 118560. http://dx.doi.org/10.1016/j.energy.2020.118560, URL https://www.sciencedirect.com/science/article/pii/S0360544220316686.

Munkejord, S.T., Bernstone, C., Clausen, S., de Koeijer, G., Mølnvik, M.J., 2013. Combining thermodynamic and fluid flow modelling for CO2 flow assurance. Energy Procedia 37, 2904–2913. http://dx.doi.org/10.1016/j.egypro.2013.06.176, URL https://www.sciencedirect.com/science/article/pii/S1876610213004190, GHGT-11 Proceedings of the 11th International Conference on Greenhouse Gas Control Technologies, 18-22 November 2012, Kyoto, Japan.

Munkejord, S.T., Hammer, M., 2015. Depressurization of CO2-rich mixtures in pipes: Two-phase flow modelling and comparison with experiments. Int. J. Greenh. Gas Control. 37, 398–411. http://dx.doi.org/10.1016/j.ijggc.2015.03.029.

Munkejord, S.T., Hammer, M., Løvseth, S.W., 2016. CO2 transport: Data and models – a review. Appl. Energy 169, 499–523. http://dx.doi.org/10.1016/j.apenergy.2016.01.100.

Onyebuchi, V., Kolios, A., Hanak, D., Biliyok, C., Manovic, V., 2018. A systematic review of key challenges of CO2 transport via pipelines. Renew. Sustain. Energy Rev. 81, 2563–2583. http://dx.doi.org/10.1016/j.rser.2017.06.064.

Oosterkamp, A., Ramsen, J., 2008. State-of-the-art overview of CO2 pipeline transport with relevance to offshore pipelines. Polytec Report number: POL-O-2007-138-A.

Orell, A., 2005. Experimental validation of a simple model for gas–liquid slug flow in horizontal pipes. Chem. Eng. Sci. 60 (5), 1371–1381. http://dx.doi.org/10.1016/j.ces.2004.09.082, URL https://www.sciencedirect.com/science/article/pii/S000925090400778X.

Orr, F.M., Taber, J.J., 1984. Use of carbon dioxide in enhanced oil recovery. Science 224 (4649), 563–569. http://dx.doi.org/10.1126/science.224.4649.563, URL https://www.science.org/doi/abs/10.1126/science.224.4649.563.

Peletiri, S.P., Rahmanian, N., Mujtaba, I.M., 2018. CO2 pipeline design: A review. Energies 11 (9), http://dx.doi.org/10.3390/en11092184, URL https://www.mdpi.com/1996-1073/11/9/2184.

Peng, D.-Y., Robinson, D.B., 1976. A new two-constant equation of state. Ind. Eng. Chem. Fundam. 15 (1), 59–64. http://dx.doi.org/10.1021/i160057a011.

Pham, L.H.H.P., Rusli, R., 2016. A review of experimental and modelling methods for accidental release behaviour of high-pressurised CO2 pipelines at atmospheric environment. Process. Saf. Environ. Prot. 104, 48–84. http://dx.doi.org/10.1016/j.psep.2016.08.013.

Picchi, D., Poesio, P., 2016. A unified model to predict flow pattern transitions in horizontal and slightly inclined two-phase gas/shear-thinning fluid pipe flows. Int. J. Multiph. Flow 84, 279–291. http://dx.doi.org/10.1016/j.ijmultiphaseflow.2016.04.010, URL https://www.sciencedirect.com/science/article/pii/S0301932216300623.

Picchi, D., Strazza, D., Demori, M., Ferrari, V., Poesio, P., 2015. An experimental investigation and two-fluid model validation for dilute viscous oil in water dispersed pipe flow. Exp. Therm. Fluid Sci. 60, 28–34. http://dx.doi.org/10.1016/j.expthermflusci.2014.07.016, URL https://www.sciencedirect.com/science/article/pii/S0894177714001861.

Poling, B.E., Prausnitz, J.M., O'Connell, J.P., 2001. The properties of gases and liquids. McGraw-Hill, New York, URL http://www.worldcat.org/search?qt=worldcat_org_all&q=0070116822.

Reynolds, W.C., 1979. Thermodynamic properties in SI: Graphs, tables, and computational equations for forty substances.

Sanderse, B., Buist, J., Henkes, R., 2021. A novel pressure-free two-fluid model for one-dimensional incompressible multiphase flow. J. Comput. Phys. 426, 109919. http://dx.doi.org/10.1016/j.jcp.2020.109919, URL https://www.sciencedirect.com/science/article/pii/S0021999120306938.

Schmid, D., Verlaat, B., Petagna, P., Revellin, R., Schiffmann, J., 2022. Flow pattern observations and flow pattern map for adiabatic two-phase flow of carbon dioxide in vertical upward and downward direction. Exp. Therm. Fluid Sci. 131, 110526. http://dx.doi.org/10.1016/j.expthermflusci.2021.110526, URL https://www.sciencedirect.com/science/article/pii/S0894177721001692.

Skarsvåg, H.L., Hammer, M., Munkejord, S.T., Log, A.M., Dumoulin, S., Gruben, G., 2023. Towards an engineering tool for the prediction of running ductile fractures in CO2 pipelines. Process. Saf. Environ. Prot. 171, 667–679. http://dx.doi.org/10.1016/j.psep.2023.01.054, URL https://www.sciencedirect.com/science/article/pii/S0957582023000654.

Sobol', I., 2001. Global sensitivity indices for nonlinear mathematical models and their Monte Carlo estimates. Math. Comput. Simulation 55 (1), 271–280. http://dx.doi.org/10.1016/S0378-4754(00)00270-6.

Span, R., Wagner, W., 1996. A new equation of state for carbon dioxide covering the fluid region from the triple-point temperature to 1100 k at pressures up to 800 MPa. J. Phys. Chem. Ref. Data 25 (6), 1509–1596. http://dx.doi.org/10.1063/1.555991.

Städtke, H., 2006. Single-phase gas flow. In: Gasdynamic Aspects of Two-Phase Flow. John Wiley & Sons, Ltd, http://dx.doi.org/10.1002/9783527610242.ch2.

Sudret, B., 2008. Global sensitivity analysis using polynomial chaos expansions. Reliab. Eng. Syst. Saf. 93 (7), 964–979. http://dx.doi.org/10.1016/j.ress.2007.04.002.

Taitel, Y., Barnea, D., 1990. A consistent approach for calculating pressure drop in inclined slug flow. Chem. Eng. Sci. 45 (5), 1199–1206. http://dx.doi.org/10.1016/0009-2509(90)87113-7, URL https://www.sciencedirect.com/science/article/pii/0009250990871137.

Teh, C., Barifcani, A., Pack, D., Tade, M.O., 2015. The importance of ground temperature to a liquid carbon dioxide pipeline. Int. J. Greenh. Gas Control. 39, 463–469. http://dx.doi.org/10.1016/j.ijggc.2015.06.004, URL https://www.sciencedirect.com/science/article/pii/S1750583615002571.

Ullmann, A., Brauner, N., 2006. Closure relations for two-fluid models for two-phase stratified smooth and stratified wavy flows. Int. J. Multiph. Flow 32 (1), 82–105. http://dx.doi.org/10.1016/j.ijmultiphaseflow.2005.08.005, URL https://www.sciencedirect.com/science/article/pii/S0301932205001242.

Vitali, M., Corvaro, F., Marchetti, B., Terenzi, A., 2022. Thermodynamic challenges for CO2 pipelines design: A critical review on the effects of impurities, water content, and low temperature. Int. J. Greenh. Gas Control. 114, 103605. http://dx.doi.org/10.1016/j.ijggc.2022.103605.

Wallis, G., 1969. One-dimensional Two-phase Flow. McGraw-Hill, URL https://books.google.it/books?id=xvFQAAAAMAAJ.

Witkowski, A., Rusin, A., aw Majkut, M., Rulik, S., Stolecka, K., 2013. Comprehensive analysis of pipeline transportation systems for CO2 sequestration. Thermodynamics and safety problems. Energy Convers. Manage. 76, 665–673. http://dx.doi.org/10.1016/j.enconman.2013.07.087, URL https://www.sciencedirect.com/science/article/pii/S0196890413004664.

Xiu, D., Karniadakis, G.E., 2002. The Wiener–Askey polynomial chaos for stochastic differential equations. SIAM J. Sci. Comput. 24 (2), 619–644. http://dx.doi.org/10.1137/s1064827501387826.

Yu, W., Lashgari, H.R., Wu, K., Sepehrnoori, K., 2015. CO2 injection for enhanced oil recovery in bakken tight oil reservoirs. Fuel 159, 354–363. http://dx.doi.org/10.1016/j.fuel.2015.06.092, URL https://www.sciencedirect.com/science/article/pii/S0016236115006729.

Yun, R., Kim, Y., 2004. Flow regimes for horizontal two-phase flow of CO2 in a heated narrow rectangular channel. Int. J. Multiph. Flow 30 (10), 1259–1270. http://dx.doi.org/10.1016/j.ijmultiphaseflow.2004.07.003, URL https://www.sciencedirect.com/science/article/pii/S0301932204001077.

Zhang, Y., Jackson, C., Krevor, S., 2022. An estimate of the amount of geological CO2 storage over the period of 1996–2020. Environ. Sci. Technol. Lett. 9 (8), 693–698. http://dx.doi.org/10.1021/acs.estlett.2c00296.

Zhang, Z., Wang, G., Massarotto, P., Rudolph, V., 2006. Optimization of pipeline transport for CO2 sequestration. Energy Convers. Manage. 47 (6), 702–715. http://dx.doi.org/10.1016/j.enconman.2005.06.001, URL https://www.sciencedirect.com/science/article/pii/S0196890405001561.